Acta Neuropathologica
https://doi.org/10.1007/s00401-021-02320-4

ORIGINAL PAPER

Clinical and neuropathological diversity of tauopathy in *MAPT* duplication carriers

David Wallon[1] · Susana Boluda[2,3] · Anne Rovelet-Lecrux[4] · Manon Thierry[2,3] · Julien Lagarde[5,6,7] · Laetitia Miguel[4] · Magalie Lecourtois[4] · Antoine Bonnevalle[1] · Marie Sarazin[5,6,7] · Michel Bottlaender[7,8] · Mathieu Mula[3] · Serge Marty[2] · Natsuko Nakamura[2] · Catherine Schramm[4] · François Sellal[9] · Thérèse Jonveaux[10] · Camille Heitz[11] · Isabelle Le Ber[12,13] · Stéphane Epelbaum[14,15] · Eloi Magnin[14,15] · Aline Zarea[1] · Stéphane Rousseau[4] · Olivier Quenez[4] · Didier Hannequin[1] · Florence Clavaguera[2] · Dominique Campion[4] · Charles Duyckaerts[2,3] · Gaël Nicolas[4]

Received: 5 January 2021 / Revised: 28 April 2021 / Accepted: 28 April 2021

Abstract

Microduplications of the 17q21.31 chromosomal region encompassing the *MAPT* gene, which encodes the Tau protein, were identified in patients with a progressive disorder initially characterized by severe memory impairment with or without behavioral changes that can clinically mimic Alzheimer disease. The unique neuropathological report showed a primary tauopathy, which could not be unanimously classified in a given known subtype, showing both 4R- and 3R-tau inclusions, mainly within temporal cortical subregions and basal ganglia, without amyloid deposits. Recently, two subjects harboring the same duplication were reported with an atypical extrapyramidal syndrome and gait disorder. To decipher the phenotypic spectrum associated with *MAPT* duplications, we studied ten carriers from nine families, including two novel unrelated probands, gathering clinical ($n=10$), cerebrospinal fluid ($n=6$), MRI ($n=8$), dopamine transporter scan ($n=4$), functional ($n=5$), amyloid ($n=3$) and Tau-tracer ($n=2$) PET imaging data as well as neuropathological examination ($n=4$). Ages at onset ranged from 37 to 57 years, with prominent episodic memory impairment in 8/10 patients, associated with behavioral changes in four, while two patients showed atypical extrapyramidal syndrome with gait disorder at presentation, including one with associated cognitive deficits. Amyloid imaging was negative but Tau imaging showed significant deposits mainly in both mesiotemporal cortex. Dopaminergic denervation was found in 4/4 patients, including three without extrapyramidal symptoms. Neuropathological examination exclusively showed Tau-immunoreactive lesions. Distribution, aspect and 4R/3R tau aggregates composition suggested a spectrum from predominantly 3R, mainly cortical deposits well correlating with cognitive and behavioral changes, to predominantly 4R deposits, mainly in the basal ganglia and midbrain, in patients with prominent extrapyramidal syndrome. Finally, we performed in vitro seeding experiments in HEK-biosensor cells. Morphological features of aggregates induced by homogenates of three *MAPT* duplication carriers showed dense/granular ratios graduating between those induced by homogenates of a Pick disease and a progressive supranuclear palsy cases. These results suggest that *MAPT* duplication causes a primary tauopathy associated with diverse clinical and neuropathological features.

Keywords Tau · MAPT duplication · Progressive supranuclear palsy · Pick disease · Tau seeding

Introduction

The *MAPT* gene encodes tau, a microtubule binding protein, which forms pathological cellular aggregates in several neurodegenerative disorders termed tauopathies [14, 20]. In primary tauopathies, tau is the driving pathological factor whereas in secondary tauopathies such as Alzheimer Disease (AD), the pathological process is associated with the interaction of tau with other proteins

David Wallon, Susana Boluda contributed equally.

✉ David Wallon
david.wallon@chu-rouen.fr

✉ Gaël Nicolas
gaelnicolas@hotmail.com

Extended author information available on the last page of the article

Published online: 06 June 2021

or peptides, namely the Aβ peptide in AD. Additionally, tauopathies can be divided into 3R, 4R or mixed subtypes according to the isoforms that accumulate. The *MAPT* messenger RNA can be alternatively spliced resulting in six isoforms of the tau protein. 4R-tau refers to tau isoforms including four microtubule-binding repeats whereas 3R-tau includes only three repeats due to the splicing out of *MAPT* exon 10 [14].

The 17q21.31 microduplication is a rare recurrent rearrangement involving four genes *(CRHR1, MAPT, STH* and *KANSL1*) which causes a recently recognized neurodegenerative disorder with poorly defined phenotypic features [15]. Among the first few cases initially reported, a constant clinical feature was severe memory impairment, associated in some cases with behavioral changes leading either to a clinical diagnosis of typical Alzheimer disease (AD) phenotype or behavioral variant of Alzheimer disease [1, 12, 15, 21]. In a previous report, we found that the cerebrospinal (CSF) biomarkers profile of the 17q21.31 duplication was consistent with an AD diagnosis in 3/4 patients, including tau-related neurodegenerative processes and abnormal amyloid β (Aβ) levels. However, amyloid positron emission tomography (PET) imaging did not support this conclusion [15]. So far, detailed neuropathological examination has been published only for one patient [1]. This case showed a marked atrophy of the frontal and the temporal lobes, hippocampus, amygdala, and a depigmentation of the substantia nigra. Immunostaining for Aβ and α-synuclein remained negative in all regions examined. The most prominent neuropathological alterations were 4R-tau inclusions, although 3R-tau positive neurofibrillary tangles were also observed in the hippocampus, entorhinal cortex, striatum, nucleus basalis of Meynert and substantia nigra. Despite its clinical presentation and CSF biomarkers profile in some patients, the 17q21.31 duplication thus appears to cause a pure tauopathy. The main pathophysiological mechanism associated with this duplication is a 1.6–1.9 fold increase of the *MAPT* messenger RNA as measured in blood samples of duplication carriers [15], presumably increasing tau protein levels. To further complicate the matter, it has recently been reported that this duplication was present in two subjects clinically diagnosed with a different phenotype, *i.e.,* atypical extra-pyramidal syndrome with gait disorder [4]. However, the in-depth description of neuropathological findings in those last two cases was not reported. In the present article, we describe novel cases, reanalyze the previously published cases with additional imaging and CSF data and report the detailed results of four neuropathological examinations.

Methods

Cases

Eight demented cases with an *MAPT* microduplication collected from year 2009 to 2019 by our laboratory were studied. Six cases were previously published [15, 21]. For two of those six cases, we add here neuropathological data that were not available at the time and updated clinical and paraclinical information. Two additional unpublished cases were identified in the meantime and added to this series. Finally, two cases, enrolled in a series of extrapyramidal syndromes, were previously published without neuropathological details [4], which we are providing here.

All patients (or legal representatives) gave informed, written consent for genetic analyses. All patients underwent a comprehensive clinical examination including personal medical and family history, neurological examination, neuropsychological assessment and, for some, lumbar puncture with CSF biomarkers analysis. Structural Magnetic Resonance Imaging (MRI), ^{123}I-Ioflupane Dopamine Transporter Single Photon Emission Computerized Tomography (Datscans) and ^{18}Fluoro-deoxyglucose (FDG) Positron Emission Tomography (PET) or Single-Photon Emission Computed Tomography (SPECT) with hexamethyl-propylene-amine-oxime (HMPAO) imaging were collected when performed as well as Amyloid and Tau-PET cerebral imaging (see details below). We collected clinical and paraclinical information from medical charts of all participants. Autopsies for cases were performed with the authorization of the patient himself or the next of keen. Cases ALZ_441_005 and ALZ_596_006 were obtained through the French national brain bank network, Neuro-CEB. We certify that the study was performed in accordance with the ethical standards as laid down in the 1964 Declaration of Helsinki and its later amendments.

Genetic analyses

Copy Number Variants (CNVs) were identified from whole exome sequencing data and confirmed by quantitative multiplex PCR of short fluorescent fragments (QMPSF) as previously described [15], except for the two additional cases identified by DNA chips (SNP array genotyping) and validated by qPCR [4]. H1/H2 *MAPT* haplotypes genotyping was determined by SNaPshot experiments using the rs1052553 single nucleotide polymorphism as a tag. Sub-haplotypes could not be determined because, in most individuals, it was not possible to unambiguously phase the polymorphisms used to tag these sub-haplotypes.

Exon 10 and at least 20 bp of the surrounding splicing regions were re-sequenced with the Sanger technique using specific primers (available upon request).

CSF biomarker analysis

CSF biomarker analyses were carried out in six different laboratories as part of the diagnostic workup using a standardized procedure. CSF samples were obtained using a Sprotte needle and collected in polypropylene tubes. They were aliquoted after centrifugation into polypropylene Eppendorf tubes, then frozen at − 80 °C within 1 h. $A\beta_{42}$, Tau (total-tau protein), and P-Tau (phosphorylated-tau protein in position 181) measurements were performed using an enzyme-linked immunosorbent assay (ELISA) (Fujirebio) according to the manufacturer's instructions. The analysis of all biomarkers was performed in two runs and averaged for statistical analyses. The quality of the results was ensured by the use of validated standard operating procedures and internal quality controls (QC) as all centers were already involved in nationwide studies. The following cut-offs were used: $A\beta_{42} < 550$ pg/mL, Tau > 350 pg/mL, P-Tau < 60 pg/mL. When $A\beta_{40}$ was available, the normal $A\beta_{42}/A\beta_{40}$ ratio cut-off was > 0.05.

Cerebral imaging data

When available, MRI scans were assessed using native DICOM format images. The presence of a cortical atrophy was evaluated; hippocampal atrophy was bilaterally scored following Scheltens visual rating scale [24]. Cortical functional imaging was assessed to identify focal hypometabolism using ^{18}FDG-PET or hypoperfusion using HMPAO-SPECT. Available DaTscan interpretations of trained nuclear physicians were used to confirm or identify dopaminergic denervation.

Amyloid and Tau PET imaging

Amyloid-β PET imaging of three patients was performed using [^{18}F]-florbetapir ($n = 1$), [^{18}F]-florbetaben ($n = 1$) or [^{18}F]-flutemetamol ($n = 1$) as previously described [15]. Tau-PET examination was performed in 2 patients (and compared to 13 already available control subjects, mean age = 68.8 years [64–75]) on a High-Resolution Research Tomograph (HRRT; CTI/Siemens Molecular Imaging). The acquisition was performed from 80 to 100 min after intravenous administration of 382 ± 11.3 MBq of [^{18}F]-flortaucipir. Dynamic list mode acquisitions were binned into successive 5-min time frames. Parametric images were created using BrainVisa software (http://brainvisa.info) by averaging the original 5-min images over 80–100 min after administration of flortaucipir. Standard Uptake Value ratio (SUVr) parametric images were obtained by dividing each voxel by the average value of the cerebellar grey matter region-of-interest with an erosion of 4 mm. Seventy-six cortical volumes of interest (VOI) were defined based on individual MRI scans and then applied onto the subject's PET space following coregistration. The VOIs, defined separately for the left and right hemispheres, were pooled into broader anatomical volumes of interest: we considered three cortical VOIs on the left and right sides respectively encompassing the temporal (with its parahippocampal, fusiform and polar sub-regions), parietal and frontal lobes.

Neuropathological examination

For each autopsy case, one hemisphere was fixed in formalin (fixation times between 8 and 27 months) and the contralateral hemisphere was frozen at -80 °C, except for case EXT_2000_001 in which the whole brain was fixed in formalin. Immunostaining was performed with the Benchmark station automated system (Ventana Medical system Inc., Roche) using the following antibodies: anti-phospho-tau (pS202,pT205): clone AT8 (mouse monoclonal, ThermoFischer, 1/500); anti 3R-Tau (RD3): clone 8E6/C11 (mouse monoclonal, Merck, 1/100); anti 4R-Tau (RD4): clone1E1/A6 (mouse monoclonal, Merck, 1/50), anti phospho-tau (pT212,pS214): clone AT100 (mouse monoclonal, ThermoFischer, 1/500), anti p-62: clone 3/P62 lck ligand (mouse monoclonal, BD Biosciences, 1/500), anti-Aβ antibody: clone 6F/3D (mouse monoclonal, Agilent, 1/200); anti-TDP43 (rabbit polyclonal, Proteintech, 1/1,000); anti α-synuclein: clone 5G4 (mouse monoclonal, Millipore, 1/4,000). Except immunohistochemistry with the Aβ and p62 antibodies, tissue was pretreated using a buffer at pH8 at 95 °C between 8 min and 1 h before adding the antibodies. The antibodies were incubated at 37 °C between 32 min and 2 h. The antigen retrieval used for Aβ was 5 min in formic acid and incubation of the antibody overnight at room temperature. For p62, the antigen retrieval was done in a buffer at pH 6 for 76 min and incubation of the primary antibody for 96 min at 37 °C. Gallyas and Bielschowsky silver techniques were used to assess argyrophilic properties of tau aggregates [29, 30].

Aβ oligomers were extracted from frontal cortex following Lesné et al. procedures [16] and analyzed by Western blot using WO2 antibody (Covance, Princeton, NJ).

Molecular profiles of tau aggregates were analyzed from sarkosyl-insoluble fraction following the protocol described by Sahara and Kimura [22] for patients ALZ_441_005 and ALZ _596_006 using brain samples extracted from frontal cortex and striatum. A patient with Pick's disease (PiD), an AD patient and a control individual were processed in parallel. Sarkosyl-insoluble fractions from patient EXT_1998_001 and a subject with progressive supranuclear

palsy (PSP) were obtained following the protocol described by Dan et al. [6]. Indeed, the protocol from Sahara and Kimura did not enable us to obtain sufficient amounts of sarkosyl-extractable aggregates for EXT_1998_001. Hence, we observed a slightly different staining for patient EXT_1998_001; notably, the 3R staining revealed several bands from lower molecular weight, which were not observed for the other patients. For the sake of comparison, the AD patient and the control individual were also extracted with this method. Sarkosyl-insoluble fractions were analyzed by Western blot using the following antibodies: anti Phospho-tau (pT181) antibody: AT270 (mouse monoclonal, ThermoFischer, 1/200), anti 3R-Tau (RD3): clone 8E6/C11 (mouse monoclonal, Merck, 1/1,000), anti 4R-Tau (RD4): clone1E1/A6 (mouse monoclonal, Merck, 1/200).

Quantification of the 4R/3R tau ratio from brain mRNA

The mRNA from frontal cortex and striatum of three patients carrying the *MAPT* duplication and five normal controls was extracted using RNA extraction kit (Macherey–Nagel). Reverse transcription was performed using verso cDNA kit (ThermoFisher Scientific). Then, cDNAs were PCR-amplified in a limited number of cycles, using a 6-FAM labelled F primer located on exon 9 (5´-CCCAAGTCGCCGTCTTCC-3´) and a R primer located on exon 11 (5´-TGGTTTATG ATGGATGTTGCCT-3´). This resulted in the amplification of 2 fragments of 207 and 300 bp, depending on the exclusion (3R-Tau) or inclusion (4R-Tau) of exon 10, respectively. After migration on an ABIprism 3500 automated sequencer (Applied Biosystems), the peak heights were quantified using the GeneMapper5 software to determine the 4R/3R Tau ratios.

In vitro seeding experiments

Preparation of human brain homogenates

In addition to brain tissues from ALZ_441_005, ALZ_596_006 and EXT_1998_001, three additional *post-mortem* brains, collected in a brain donation project and stored in the French national brain biobank (Bioressource Research Impact Factor number = BRIF BB-0033–00011), were used for this study: one 72-year-old male corresponding to a control case devoid of any Aβ, phospho-tau or α-synuclein accumulation, one 64-year-old female with progressive supranuclear palsy (PSP case) and one 61-year-old male with Pick's disease (PiD case). The following samples were chosen: striatum of the three *MAPT* duplication cases, pons of the PSP case (as example of a 4R tauopathy) and frontal cortex of the PiD case (as example of a 3R tauopathy). The striatum of the control case was also studied. Approximately 150 mg of frozen tissue were thawed on ice and mixed with ice-cold phosphate-buffered saline (PBS) containing protease and phosphatase inhibitor cocktail (Thermo Fisher Scientific), to reach a final solution of 20% weight/volume. Tissue was homogenized by 15–20 strokes in a 1 mL glass homogenizer (Fisher Scientific), briefly sonicated on ice with a Misonix Q125 sonicator (Q-sonica) and clarified by centrifugation (3000 g, 5 min, 4 °C), as previously described [27]. Supernatants were collected, aliquoted and stored at − 80 °C. Concentrations of tau proteins were assessed by total tau (Total) Human ELISA Kit (Invitrogen, Thermo Fisher Scientific).

Treatment of biosensor cells sensitive to tau seeding

The seeding activity of each homogenate was evaluated on a misfolded tau biosensor (HEK cells expressing tau RD P301S coupled with YFP or CFP fluorochromes, #CRL-3275, ATCC, LGC Standards). Those cells were plated in 24-well plates and treated in duplicate, following the original protocol adapted at the laboratory [9, 11], with a few adjustments. A transduction mix was prepared with 43.75 µL Opti-MEM (Gibco, Thermo Fisher Scientific) and 6.25 µL Lipofectamine 2000 (Invitrogen, Thermo Fisher Scientific), combined with 50 µl of the homogenate diluted in Opti-MEM and normalized by total tau. The transduction mix was briefly spun, incubated for 30 min at room temperature and added to the cells. Cells were left in the incubator during 24 h. The experiment was replicated three times.

Analysis

Treated cells were re-plated on 13 mm diameter coverslips coated with poly-D-lysine (Sigma-Aldrich) and left 6-7 h in the incubator. Cells were fixed in 4% PFA and counterstained with DAPI. The coverslips were mounted with Fluoromount (Sigma-Aldrich). Slides were stored in the dark at 4 °C until observation with an inverted confocal Leica TCS SP8 DLS (Leica Microsystems). The YFP/CFP positive cells were manually counted from max intensity projection images (four microscopic fields per coverslip, eight per condition). The morphology profiles of YFP/CFP positive aggregates were assessed from stack images (50 ± 10 aggregates per condition).

Results

In addition to the six 17q21.31 duplication carriers already reported by our group [15, 21], and the two reported in the Chen et al. paper [4], we have identified two unrelated novel cases carrying the same rearrangement, leading to a total of ten cases from nine families. In all cases, the size

of the duplicated segment was identical and encompassed the entire *MAPT* coding sequence. As displayed in Table 1, these microduplications occurred in different H1/H2 haplotypic backgrounds.

Clinical features

Clinical phenotypes of all ten carriers are summarized in Table 1. Mean age of onset was 51.3 years (range: [37–57]) with 6/10 being male patients. In eight cases, an amnestic syndrome was the main clinical phenotype. Among them, four patients initially showed exclusive memory impairment, three presented with memory loss associated with either apathy or other behavioral disturbances and one first exhibited behavioral disorder and then memory impairment. The cognitive follow-up of seven patients including a verbal episodic memory assessment by the Free and Cued Selective Reminding Test, revealed a hippocampal dysfunction defined as an abnormal free recall without normalization of the cued retrieval [23]. On the remaining cognitive domains, behavioral and cognitive dysexecutive syndromes (following criteria available at Ref. [10]) were identified for six patients. Accordingly, the verbal fluency was in abnormal ranges in all of them. None of them presented with visuoperceptual impairment. Neurological examination of these eight patients was otherwise unremarkable at first visit. In particular, there was not any motor, sensitive, pyramidal tract or extrapyramidal signs. No vertical gaze palsy was noticed. All of them gradually declined towards a severe memory deficit with misorientation and gesture apraxia inducing a progressive impact on instrumental activities of their daily living.

Both cases with an initial akinetic-rigid syndrome developed gait disorders with falls associated with dysarthria, resting tremor and genito-urinary dysfunction. Symptoms were considered levodopa moderately sensitive in EXT_2000_001 and levodopa-resistant in EXT_1998_001. No vertical gaze palsy was reported for EXT_1998_001; it was noted only during the last year before death of EXT_2000_001. In this last patient, executive and attention deficits with judgment impairment and perseverative ideas were reported after a time course of 5 years (1 year before death). Unfortunately, no detailed cognitive assessment was available for this patient. In patient EXT_1998_001, a memory impairment was present at first examination and progressively worsened, 4 years after onset of motor signs and 3 years before death (MMSE scored 23/30 at year 4 and MMSE scored 17/30 with complete temporal disorientation at year 5). Due to these unusual clinical presentations, main clinical hypotheses during the follow-up of both patients were first multiple system atrophy with predominant parkinsonism and then atypical progressive supranuclear palsy (PSP).

Among this group of *MAPT* duplication carriers, at the present time, five patients have died from their disease. Autopsies were available in four of them. Mean disease duration was 10.1 years [5–20] when considering the whole group of carriers and 12.0 years when restricting to deceased patients.

CSF biomarkers

As can be seen in Table 1, CSF tau and p-tau values were in the abnormal ranges while CSF Aβ was normal in the two novel patients (EXT_1593_001 and EXT_1687_001). In one previously reported individual (ALZ_596_001) with an $A\beta_{42}$ value below the threshold, a second CSF biomarker assessment following a novel lumbar puncture (4 years after the first one) showed an $A\beta_{42}$ value in the normal range (646 pg/mL). Overall, CSF $A\beta_{42}$ values were considered in the normal ranges in 4/6 patients tested.

Brain imaging patterns (MRI, FDG-PET, DAT-SCAN)

MRI scans, performed between 1 and 5 years after disease onset, were available for eight patients. White matter hyperintensities on FLAIR-weighted images were present in 3/8 patients but were mild, punctiform and periventricular for ALZ_596_001 and EXT_1114_001 (with a medical history of vascular risk factors) or posterior, moderate and periventricular for EXT_1593_001 (who presented smoking addiction) (Fig. 1a). Cortical atrophy was present in all patients although differentially located. Internal temporal atrophy was found in all cognitively impaired patients, associated with anterior temporal atrophy in three patients (ALZ_596_001, EXT_1687_001, ALZ_441_005) or parietal and occipital atrophy in another three (EXT_1593_001, EXT_1114_001 and ROU_1373_001) (Fig. 1a–d). Conversely, no cortical atrophy was noticed for patients EXT_1998_001 and EXT_2000_001.

Functional imaging using FDG-PET or HMPAO-SPECT, showed a pattern consistent with the atrophy profiles on MRI. Tracer uptake was decreased in the temporal cortex of all five analyzed patients. The uptake was additionally decreased in the parietal regions of three patients: ROU_1373_001 (Fig. 1e), EXT_1593_001 and ALZ_441_005. Interestingly, that last patient also showed a severe frontal right hypometabolism.

DaTscans were performed in four patients. Only one of them (EXT_2000_001) presented with an extrapyramidal syndrome. The three other patients had no extrapyramidal syndrome, neither at first visit, nor at follow-up. Strikingly, all four patients showed significantly decreased uptake of the tracer, suggesting bilateral nigro-striatal dopaminergic neuronal loss, either symmetrical for ROU_1373_001 and

Table 1 Demographic, genetic, clinical, imaging and biological data of all *MAPT* duplication carriers

	ALZ_596_001	ALZ_596_006	EXT_1593_001	EXT_1114_001	ROU_1373_001	ROU_747_001	EXT_1687_001	ALZ _ 441_005	EXT_1998_001	EXT_2000_001
Published in / novel case	[15]	[15]	novel	[15]	[15]	[21]	novel	[15]	[4]	[4]
Age at onset (years)	50	55	56	57	54	49	53	45	57	37
Sex	M	M	M	F	M	F	F	M	F	M
MAPT haplotype	H1/2H2	H1/2H2	H1/2H2	H1/2H2	2H1/H2	3H1	H1/2H2	2H1/H2	H1/2H2	NA
First reported symptoms	Memory	Memory	Memory, behavior	Memory, behavior	Memory	Behavior	Memory	Behavior, memory	Akinetic–rigid synd	Akinetic–rigid synd
Family history of dementia	+ (same family as ALZ_596_006)	+ (same family as ALZ_596_001)	+	+	–	+	+	– (de novo mutation)		
Extrapyramidal syndrome at onset	–	–	–	–	–	–	–	–	+	+
Behavioral or cognitive dysexec. synd	–		+	+	–	+	–	+	+	+
Visuoperceptive impairment	–		–	–	–		–	–		
Disease duration (years)	11	16 (to death)	6	8	10	20 (to death)	6	13 (to death)	6 (to death)	5 (to death)
MRI (years ADO)	5		2	1	4		3	2	4	3
Presence of WMH	+		+	+	–		–	–	–	–
Anterior temporal atrophy	+		–	–	–		+	+	–	–
Internal temporal atrophy	+		+	+	+		+	+	–	–
Scheltens score (R/L)	4–4		3–3	3–3	3–3		4–3	3–3		0–0
Frontal atrophy	–		–	–	–		–	+	–	–
Parietal/occipital atrophy	–		+	+	+		–	–	–	–

Table 1 (continued)

	ALZ_596_001	ALZ_596_006	EXT_1593_001	EXT_1114_001	ROU_1373_001	ROU_747_001	EXT_1687_001	ALZ _ 441_005	EXT_1998_001	EXT_2000_001
HMPAO-SPECT/FDG-PET (years ADO)	3		3	3	5			3		
Temporal cortex	P		P	P	P			P		
Parietal cortex	N		P	N	P			P		
Frontal cortex	N		N	N	N			P		
DaTScan (years ADO)			P (3)		**P (10)**		**P (6)**			**P (2)**
Amyloid-PET (years ADO)	N (6)			N (3)	N (4)					
Tau-PET (years ADO)	**P (8)**				**P (9)**					
CSF Biomarkers (years ADO)	3		3	3	2		2	1		
Aβ42 (pg mL^{-1})	**496** / 646[a]		1372	**372**	864		850	**260**		
Tau (pg mL^{-1})	**558 / 558**[a]		**789**	**866**	**696**		**1284**	**507**		
P-Tau (pg mL^{-1})	**66** / 56[a]		**82**	**94**	**98**		12	**67**		
Aβ42/Aβ40	n.a / 0.07[a]		0.16				0.06			

Empy cells is mean data are not available

+ present, − absent, *dysexec. synd.* dysexecutive syndrome, *WMH* white matter hyperintensities, *HMPAO-SPECT* hexamethylpropanolamine oxime single photon emission computed tomography, *FDG-PET* fluorodeoxyglucose positron emission tomography, *ADO* after disease onset, *R* right, *L* left, *DaTScan* dopamine transporter scan, *amyloid-PET* amyloid-tracer positron emission tomography, *tau-PET* Flortaucipir tau-tracer positron emission tomography, *CSF* cerebrospinal fluid, *Aβ42* β-amyloid 1–42 peptide, *Aβ40* β-amyloid 1–40 peptide, *P-Tau* phosphoryled-tau protein, ***P*** pathological, *N* Normal. Abnormal CSF biomarker values appear in bold. Normative values for CSF biomarkers were: Aβ42 > 550 (pg mL^{-1}), Tau < 350 (pg mL^{-1}), P-Tau < 60 (pg mL^{-1}), Aβ42/Aβ40 > 0.055

[a]Novel analysis after second lumbar puncture

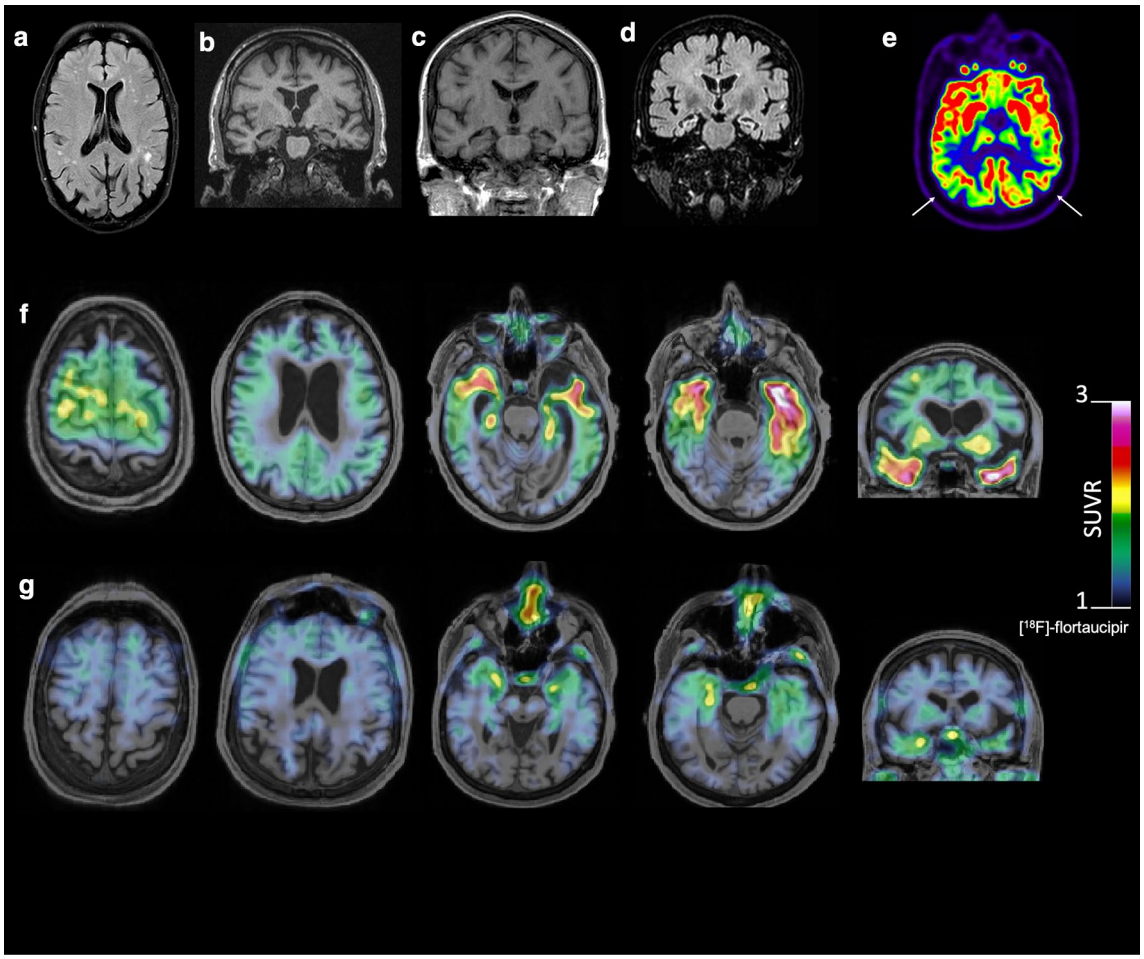

Fig. 1 Structural, functional and Tau PET Cerebral imaging of MAPT duplication carriers. **a** FLAIR-weighted axial MRI scan of EXT_1593_001 showing parietal cortical atrophy and mild white matter hyperintensities. **b** T1-weighted coronal MRI scan of EXT_1114_001. **c** T1-weighted coronal MRI scan of ROU_1373_001. **d** FLAIR-weighted sequence coronal MRI scan of EXT_1687_001. **e** FDG-PET scan of ROU_1373_001 showing parietal bilateral hypometabolism (arrows). **f** Tau-PET imaging of ALZ_596_001 with color scale corresponding to the SUVR scale. **g** Tau-PET imaging of ROU_1373_001 with color scale corresponding to the SUVR scale

EXT_2000_001, or asymmetrical for EXT 1593_001 and EXT_1687_001 (left predominance for both).

Molecular imaging

Amyloid PET was available in three patients (already reported in [15]) including in patient ALZ_596_001 with initially low and then normal CSF $A\beta_{42}$ values, and in patient EXT_1114_001 with abnormal $A\beta_{42}$ values. Amyloid PET scans were all considered as normal (Table 1).

Tau-PET imaging using [^{18}F]-flortaucipir was performed in two patients. On visual inspection, we found that the tracer binding, 8 years after disease onset, was strongly increased in the temporal lobes and in the posterior and superior region of the frontal lobes of ALZ_596_001 (Fig. 1f). The other patient (ROU_1373_001) had less pronounced [^{18}F]-flortaucipir binding on the imaging performed 9 years after onset. The uptake was restricted to the medial and anterior temporal regions. A control group of 13 individuals was used to calculate the mean and the standard deviation (SD) of the SUVRs in the regions of interest. The SUVRs of ALZ 596_001 were above mean plus 1.96 SD of controls (95% confidence interval), in the temporal lobes (parahippocampal, fusiform, inferior temporal and temporo-polar regions), as well as in the supplementary motor areas. In patient ROU

1373_001, only the parahippocampal gyri and right temporal pole were above mean plus 1.96 SD (Fig. 1g).

Neuropathological findings

Neuropathological findings are summarized in Figs. 2, 3, Table 2, Supplementary Fig. 1, supplementary Fig. 2, Supplementary Fig. 3, Table 2 and supplementary Table 1.

ALZ_441_005

At autopsy, the brain was extremely atrophic, the left hemisphere weighted 347 g after formalin fixation. Macroscopic examination of the left hemisphere revealed a severe atrophy of the frontal, temporal and parietal lobes, mostly affecting the association cortices. The striatum was also atrophic, in particular the caudate nucleus. The hippocampus and amygdala were barely identifiable (Supplementary Fig. 1a, b). The brainstem also showed a generalized atrophy. There was a loss of pigment of the *substantia nigra* and the *locus cæruleus* was not identifiable. Finally, in the cerebellum, in addition to a chronic cavitary infarction of the left hemisphere, there was an atrophy of the dentate nucleus.

Histology revealed massive neuronal loss, severe astrogliosis and marked spongiosis in the regions where atrophy was seen at macroscopic examination. These neurodegenerative changes were associated with severe degeneration of the adjacent subcortical white matter.

Immunohistochemistry using the AT8 anti-tau antibody revealed a great number of hyperphosphorylated tau deposits in neurons, astrocytes and less frequently in oligodendrocytes as well as in the neuropil. Tau positive aggregates were numerous and seen predominantly in the neocortex, striatum, pallidum, limbic regions, including the hippocampus and entorhinal cortex (Figs. 2a, b, 3) and the cerebellum. Neocortical pathology involved the frontal, temporal and parietal lobes with very little tau pathology in the occipital cortex. Tau pathology predominated in the grey matter and was scant to moderate in the white matter. In the brainstem, AT8-positive aggregates were numerous in the midbrain and the pons but not in the medulla oblongata. In neurons, the majority of the deposits were spherical inclusions reminiscent of Pick bodies (Fig. 2a). However, although the aggregates were mainly 3R-tau, a significant number of inclusions were also 4R-tau immunoreactive. The inclusions did not show argyrophilic properties with the Bielschowsky silver staining, except for a few neurons in the dentate gyrus and CA1 regions of the hippocampus, but were positive for Gallyas silver staining (Supplementary Table 1). Neurons with diffuse cytoplasmic neuronal immunoreactivity or globose neurofibrillary tangles (NFTs) were also observed but in a much lesser number. In the dentate nucleus of the cerebellum, coarse grain intracytoplasmic neuronal inclusions predominated (Supplementary Fig. 2). The astrocytic deposits reminded of ramified astrocytes as in Pick's disease (PiD) (Fig. 2a). They showed tau positivity close to the nucleus and lacked fine prolongations in the astrocytic processes. Of note was the predominance of neuronal intracytoplasmic spherical inclusions and neuropil threads (NTs) with very few glial lesions seen in the striatum (Fig. 2b). Aggregates in oligodendrocytes were not numerous and they were predominant in the white matter of affected regions. Small round spherical inclusions, smaller than the nuclei, similar to those seen in Pick disease, were more abundant than coiled bodies (Supplementary Figs. 2 and 3).

Tau aggregates in neurons and astrocytes were labeled with 3R-tau and 4R-tau whereas oligodendrocytes were labelled with 3R-tau and less frequently with 4R-tau. As can be seen in Table 2 summarizing the presence of 3R and 4R-tau deposits among nine brain regions in each available autopsy case, there was a predominance of 3R-tau isoforms over 4R isoforms in neurons and astrocytes of all examined brain regions. It is noteworthy that the striatal neuronal deposits were strictly labeled by 3R but not 4R-tau (Fig. 2b). Neuronal, astroglial and oligodendrocytic aggregates were immunoreactive for p62 and AT100. Argentophilic properties were variable depending on the region. A few neuronal globular deposits showed argyrophilia with Bielschowsky staining in the dentate gyrus of the hippocampus while they were negative for Gallyas, as seen in PiD (Supplementary Fig. 3c). However, in the frontal cortex and striatum, they were positive for Gallyas and negative for Bielschowsky silver staining. Small globular oligodendroglial deposits in the white matter showed argyrophilic properties both with the Gallyas and Bielschowsky stainings (Supplementary Fig. 3b).

Sarkosyl-insoluble fractions from the frontal cortex and striatum blotted with phospho-tau antibody revealed two main bands at 55 and 64 kDa, similar to the pattern observed in a PiD case processed in parallel. Consistently, when blotted with a 3R-tau antibody, these western blots showed intense immunoreactivity whereas no immunoreactivity was detected with the 4R-tau-specific antibody (Fig. 4a).

Overall, the morphology of tau aggregates was reminiscent of that observed in PiD. However, immunohistochemical and argyrophilic properties of the aggregates showed some differences. There was abundant pathology in the dentate nucleus of the cerebellum, which is not usually observed in PiD. Furthermore, white matter pathology was scant and the globular oligodendroglial aggregates were of small size compared to the ones seen in globular glial tauopathy.

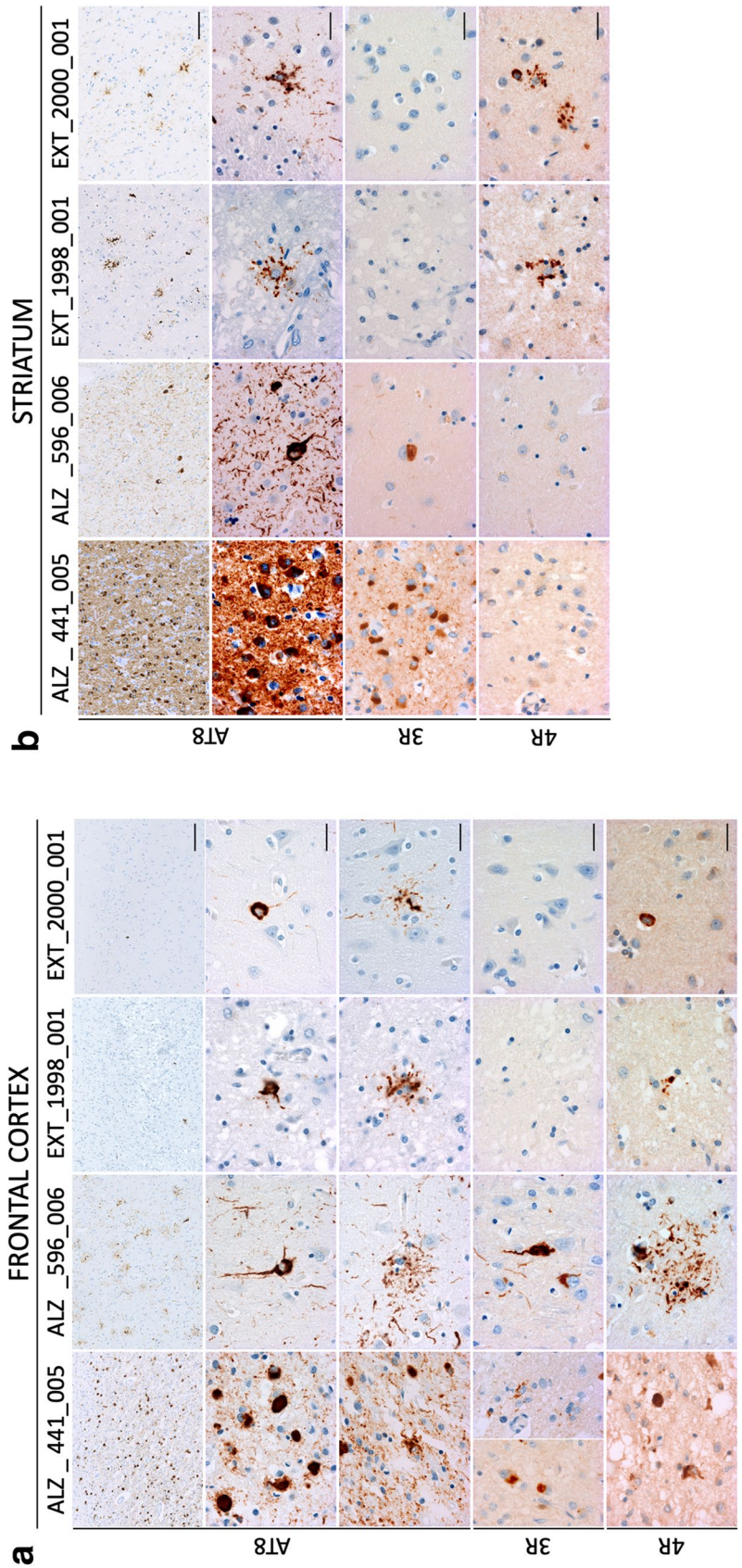

Fig. 2 Tau pathology of the four cases carrying a *MAPT* duplication in the frontal cerebral cortex (a) and the caudate nucleus (b). **a** Diversity of tau pathology and 3R- and 4R-tau isoform expression in the frontal cortex. In ALZ_441_005, pathology was abundant with a predominance of neuronal deposits with many globular Pick-like bodies in the neurons. Astrocytic deposits were also numerous and reminded of ramified astrocytes with deposits close to the nucleus and without the ramifications. In ALZ_596_006, there was a predominance of astrocytic pathology with many tufted astrocytes and some neurofibrillary tangles (NFTs) in neurons. Tau pathology in EXT_1998_001 and EXT_2000_001 was scant and only a few deposits in the form of tufted astrocytes and a few NFTs in neurons were seen. Tau aggregates in ALZ_441_005 and ALZ_596_006 included the 3R- and 4R-tau isoforms. EXT_1998_001 and EXT_2000_001 tau aggregates expressed solely 4R-tau. Frontal cortex. Immunohistochemistry: AT8, 3R-tau, 4R-tau. Scale bar in first row 100 µm, Scale bar in four last rows 25 µm. **b** Diversity of tau pathology and 3R- and 4R-tau isoform expression in the caudate nucleus. In ALZ_441_005, pathology was abundant with a predominance of neuronal pathology with many globular Pick-like bodies in neuronal soma and abundant neuropil threads. In ALZ_596_006 neuropil threads were many, however neuronal neurofibrillary tangles (NFT) were moderate in number. In EXT_1998_001 and EXT_2000_001, pathology was predominantly astroglial with astrocytic deposits resembling tufted astrocytes. ALZ_441_005 and ALZ_596_006 expressed only 3R-tau isoforms and EXT_1998_001 and EXT_2000_001 were positive only for 4R-tau immmunohistochemistry. Caudate nucleus. Immunohistochemistry: AT8, 3R-tau, 4R-tau. Scale bar in first row 100 µm, Scale bar in last three rows 25 µm

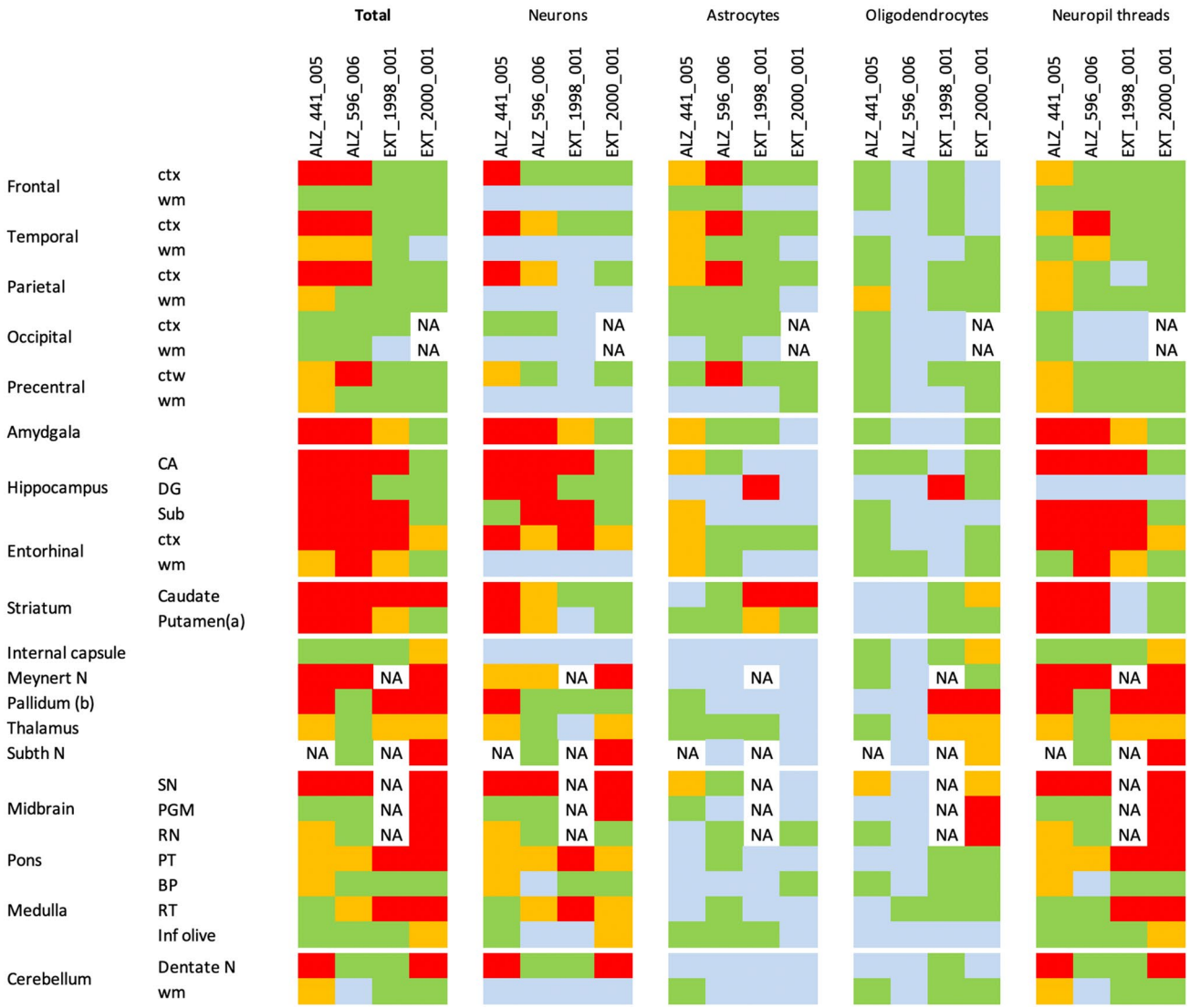

Fig. 3 Distribution and intensity of tau pathology in the brain of *MAPT* duplication carriers. Color-coded table following a quantitative evaluation of tau pathology per cerebral region. Semiquantification of total tau pathology (total) in neurons, astrocytes, oligodendrocytes and neuropil (neuropil threads) in relevant brain regions. Blue = 0; Green = rare or scant; Orange = moderate; Red = abundant. *NA* not available. (**a**) Tau pathology is seen in the anterior part of the putamen in case ALZ_596_006 and EXT_1998_001. (**b**) Tau pathology only involves the external pallidum in case ALZ_441_005. *BP* basis pontis, *CA* cornu Ammonis, *ctx* cortex, *dentate* dentate nucleus, *DG* dentate gyrus, *inf olive* inferior olive, *PGM* periventricular gray matter, *PT* pontine tegmentum, *RN* red nucleus, *RT* reticular formation, *SN* substantia nigra, *Sub* subiculum, *Subth* subthalamic nucleus, *wm* white matter

ALZ_596_006

The fixed left hemisphere weighted 587 g. Macroscopic examination revealed a moderate atrophy of the medial region of the temporal lobe associated to a moderate ventricular dilatation (Supplementary Fig. 1c).

Histology showed marked neuronal loss associated with reactive gliosis in the amygdala, the hippocampus and the entorhinal cortex. A mild to moderate neuronal loss was seen in the nucleus basalis of Meynert, the *substantia nigra* and the *locus cæruleus*. The cerebellum appeared intact at hematoxylin and eosin (H&E) examination.

Immunohistochemistry revealed marked tau pathology in the neocortex where there was a predominance of tau positive astrocytes, with moderate number of NFTs and NTs (Fig. 2a). Tau deposits in the astrocytes had various morphologies: some accumulated tau near the nucleus, others had fine deposits in the distal part of the processes and in others the deposits were seen along the length of the processes. In the striatum, the number of tau aggregates was moderate and involved the neurons with the presence of

Table 2 Distribution of 4R and 3R aggregates among brain regions in *MAPT* duplication carriers (patients ordered from right to left based on the main aggregated tau isoforms)

	ALZ_441_005	ALZ_596_006	EXT_1998_001	Case III-2 of [1]	EXT_2000_001
Frontal cortex	3R > 4R	4R > 3R[c]	4R	4R	Negative[a]
Hippocampus	3R > 4R	3R > 4R	3R/4R	3R/4R	4R[b]
Enthorhinal cortex	3R > 4R	3R > 4R	3R > 4R	3R/4R	3R/4R
Amygdala	3R > 4R	3R > 4R	3R/4R	4R > 3R	4R
Striatum	3R	3R	4R	4R > > 3R	4R
Pallidum	3R > > 4R	3R/4R	4R	4R > > 3R	4R
SN	3R > 4R	4R > 3R	ND	4R > > 3R	4R
NBM	3R > > 4R	3R > 4R	3R/4R	3R/4R	4R
Cerebellum	NA	3R/4R	4R	4R	4R

3R: positive immunostaining of 3R tau protein isoforms; 4R: positive immunostaining of 4R tau proteins isoforms. Case III-2 of [1]: immunohistochemistry data from the published case by Alexander et al. [1]

NA not available

[a]Negative: rare AT8-positive deposits which were negative for 3R and 4R staining

[b]4R: rare AT8-positive deposits which were negative for 3R staining

[c]4R > 3R: In the frontal cortex, 3R and 4R were similar in neurons but astrocytes were only positive for 4R

many NFTs and NTs (Fig. 2b). Very few tau positive astrocytes were seen in the striatum (Fig. 3). Tau pathology in the pallidum was rare (Supplementary Fig. 2). In the brainstem, tau pathology was abundant in the *substantia nigra*, which showed many globose NFTs and NTs (Supplementary Fig. 2). In the pons, tau deposits were observed mainly in the tegmentum, including the *locus cœruleus*. Both neuronal and astrocytic deposits were seen. In the medulla oblongata, tau pathology predominated in the reticular formation. The cerebellum had very few aggregates in the dentate nucleus (Supplementary Fig. 2). Oligodendrocytes were only observed in the reticular formation of the medulla and the amygdala. Subependymal, perivascular and subpial thorny astrocytes were seen in the medial region of the temporal lobe and striatum suggesting the presence of associated aging-related tau astrogliopathy (ARTAG) (Supplementary Fig. 3). A few clusters of astrocytes in the white matter of the frontal, parietal and occipital lobes were also seen. Tau pathology in the medial temporal lobe with numerous NFTs and NTs in the hippocampus, the entorhinal cortex and the amygdala were also observed (Supplementary Fig. 3). Occasional diffuse Aβ plaques were seen in the cortex. All of the deposits were positive for p62 and AT100. Neuronal aggregates were immunoreactive for 3R-tau and 4R-tau. In contrast, astrocytes where only 4R-tau positive. Silver staining was variable. Neurons and astrocytes where positive for Gallyas silver staining and only occasional neuronal aggregates and rarely astrocytes where argyrophilic with Bielschowsky (Supplementary Fig. 3). As can be seen in Table 2 and Fig. 2, when analyzed for tau isoforms, neuronal aggregates were 3R- and 4R-tau positive with a predominant 3R-tau labelling in almost all structures examined. As in case ALZ_441_005, the striatum was only immunoreactive for 3R-tau. Western blot of insoluble fractions from frontal cortex and striatum, labeled with AT270 antibody showed three bands similar to those seen in AD. The two lower bands were intensively labelled by 3R-tau while the upper and middle bands were labelled by 4R-tau (Fig. 4b).

Overall, this case shows a tauopathy (3R > 4R) that mainly involves neurons and astrocytes, in cortical and subcortical regions, in which tau aggregates adopt diverse morphologies. Distribution and biochemical properties of the lesions did not fulfill the criteria for either of the known tauopathies.

EXT_1998_001

The right hemisphere fixed in formalin weighted 391 g (brainstem and cerebellum not included). Gross examination of the coronal sections did not show atrophy of the brain parenchyma (Supplementary Fig. 1d). The study of the mesencephalon was limited, as the brainstem had been previously separated from the hemisphere through this region. However, the rest of the brainstem appeared to have a normal size at macroscopic examination. The *locus cœruleus* was not identified.

Histology showed, in addition to widespread anoxic lesions, a tauopathy involving the brainstem, pallidum, striatum, thalamus and dentate nucleus of the cerebellum. In the brainstem, the pallidum and the dentate nucleus, the most prominent AT8 positive tau inclusions were globular bodies, diffuse neuronal intracytoplasmic granular immunoreactivity and NTs (Supplementary Fig. 2). Coiled bodies were seen in the pallidum. Tufted astrocytes were the only tau pathology seen in the striatum (Fig. 2b). In the frontal cortex, the pathology was limited but the extensive laminar necrosis and massive neuronal loss could have explained the scarcity of tau deposits which were

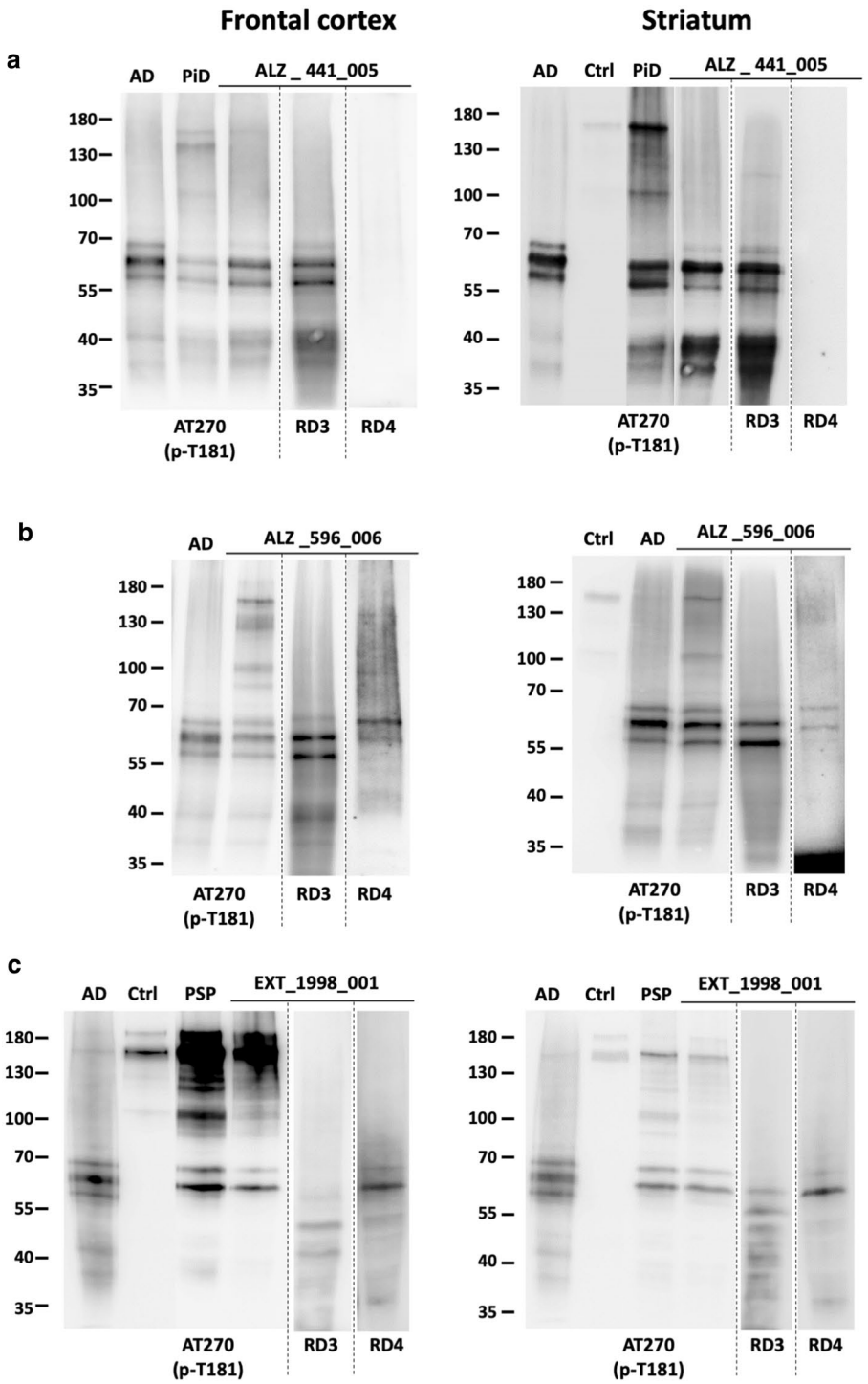

Fig. 4 Western blots of sarkosyl-insoluble 4R and 3R-Tau in patients and controls. **a** Analysis of patient ALZ_441_005; **b** Analysis of patient ALZ_596_006. **c** Analysis of patient EXT_1998_001. For all patients, western blotting was performed on brain samples extracted from frontal cortex (left panels) or striatum (right panels). Blots were revealed with antibodies against Tau phosphorylated on Thr181 (AT270 tracks), 3R-Tau (RD3 tracks) or 4R-Tau (RD4 tracks). Tau profiles obtained from the *MAPT* duplication carriers were compared to those of patients showing Alzheimer's disease (AD), Pick's disease (PiD) or PSP neuropathology, and to a control individual (Ctrl). Note that western blots are presented here as a composite image from different times of exposure of a unique blot for each panel (all samples from each panel migrated on a same blot) to better compare Tau profiles between each antibody despite varying staining intensity. Note that RD4 staining requires longer exposure than using RD3 antibody, so that minor 4R aggregates as observed in IHC may be hardly detectable in WB performed in similar regions

predominantly found in tufted astrocytes (Fig. 2a). A few NTs and coiled bodies in the subjacent white matter were seen. In the medial and lateral regions of the temporal lobe, tau pathology which included NFTs, granular intracytoplasmic aggregates, NTs and ghost tangles was severe. Immunohistochemistry for tau antibodies in the frontal cortex and striatum revealed that tau pathology was only of the 4R isoforms, while 3R-tau immunohistochemistry was negative (Fig. 2). Neuronal and astrocytic aggregates were immunoreactive for p62 and AT100. Oligodendrocytes showed frequent immunoreactivity for AT100 but it was rare for p62. Silver staining showed positivity for Gallyas while Bielschowsky was negative (Supplementary Table 1). In medial temporal brain regions, the deposits, consistent with Braak stage II-III tau pathology, were labeled with both 3R and 4R-tau (Table 2).

Sarkosyl-insoluble fraction from the frontal cortex and striatum blotted with AT270 antibody showed a two-band profile reminiscent of PSP. When blotted with a 3R-tau antibody, samples from frontal cortex did not show any immunoreactivity, while samples extracted from the striatum showed a faint, 2-band pattern, corresponding to 55 and 64 kDa Tau bands. Both samples were labeled by the 4R-tau antibody, with a similar pattern to that seen with the AT270 antibody, confirming that tau aggregated, in these regions, was mainly 4R (Fig. 4c).

EXT_2000_001

The formalin fixed whole brain weighted 1200 g. At gross examination, the *substantia nigra* was pale and the subthalamic nucleus, atrophic. There was a moderate dilation of the 3rd ventricle (Supplementary Fig. 1e). Histologic examination with hematoxylin–eosin (H-E) evidenced, in accordance with the macroscopic observations, a massive neuronal loss in the *substantia nigra*. The neuronal loss was severe in the subthalamic nucleus. The pallidum was gliotic. The neocortex and the hippocampus appeared normal.

Tau positive aggregates were mainly detected in subcortical regions (especially in the basal ganglia and in the brainstem) and were minimal in the frontal cortex and hippocampus (Fig. 2a, b; Supplementary Fig. 1). The predominant lesions were NFTs, sometimes globose, NTs and astrocytic deposits. In the astrocytes, AT8 tau positive aggregates were atypical, close to the nuclei with little ramifications. In the caudate nucleus, however, the morphology of the astrocytic aggregates was similar to that of tufted astrocytes (Fig. 2a, b). Coiled bodies in the oligodendrocytes were infrequent. In the striatum, aggregates were seen in the caudate nucleus while they were scarce in the putamen. The internal capsule was the only region that showed many coiled bodies and NTs were also frequent. Tau pathology was marked in the pallidum (Supplementary Fig. 2). While the thalamus was moderately involved the subthalamic nucleus had massive pathology with a predominance of neuronal deposits (NFTs and NTs). Mainly globose NFTs were seen in the nucleus basalis of Meynert. In the brainstem there was a large number of deposits in the *substantia nigra* and the periaqueductal grey of the mesencephalon. In the pons, tau aggregates were numerous in the tegmentum while they were rare in the ventral pons (Supplementary Fig. 2). In the medulla oblongata, the aggregates predominated in the reticular formation, in the cranial nerve nuclei and in the inferior olive, where mainly NFTs were seen. In the cerebellum, the presence of many coarsed granular neuronal intracytoplasmic aggregates and NTs in the dentate nucleus was surprising compared to its normal appearance after H-E staining. All of the tau deposits seen were positive for the 4R isoforms and negative for the 3R isoforms (Table 2, Fig. 2). In the entorhinal cortex tau aggregates expressed both 3R and 4R isoforms, consistent with Braak stage II tau pathology. As with the previous case, all of the tau aggregates were positive for AT100. P62 immunoreactivity was also seen in all types of aggregates, however it was scant compared to the amount of tau pathology seen. Similarly to the previous case, tau aggregates were positive for Gallyas and negative for Bielschowsky silver staining (Supplementary Table 1). No Western blot analysis was undertaken due to the lack of frozen tissue.

Overall, the distribution and characteristics of tau pathology in cases EXT_1998_001 and EXT_2000_001 was reminsicent of that observed in progressive supranuclear palsy (PSP) cases. However, compared to typical PSP, in our two cases, oligodendrocytes with tau pathology (coiled bodies) were scant and tau aggregates in the pontine basis were rare.

No evidence for associated proteinopathies

There was no associated α-synuclein or TDP-43 proteinopathies in any of the cases (Supplementary Fig. 7). No Aβ deposits were observed except in case ALZ_596_006 where rare diffuse Aβ plaques were seen in the cortex of the middle frontal gyrus, the subcallosal area and the inferior temporal gyrus. No Aβ oligomers were detected by western blot analysis of the frontal cortex of the three cases with available frozen tissue (Supplementary Fig. 4).

Analysis of exon 10 splicing and determination of 4R/3R tau mRNA ratios

The alternative splicing of exon 10 in mature *MAPT* mRNA naturally leads to either 3R-tau (in case of exon 10 skipping) or 4R-tau (in case of exon 10 inclusion). In an attempt to identify genetic variants influencing alternative splicing of exon 10, we sequenced exon ten boundaries in the nine cases with available DNA. No single nucleotide variant, short insertion or deletion putatively influencing splicing was found.

MAPT 4R/3R mRNA ratios were analyzed in two cerebral regions (frontal cortex and striatum) for the three patients for whom frozen tissue was available (EXT_1998_001, ALZ_596_006 and ALZ_441_005) and for five normal controls. In controls, the 4R/3R mean ratio was 0.69 ± 0.10 (SEM) in the frontal cortex and 0.97 ± 0.16 (SEM) in the striatum. For each control, the 4R/3R ratio was systematically increased in the frontal cortex compared to striatum, but this increase was collectively not significant ($p = 0.125$, Wilcoxon signed ranked test). In the frontal cortex of the patient with 3R-tau aggregates resembling Pick bodies (ALZ_441_005), we noted a 243% increase of the 4R/3R mRNA ratio as compared to the mean value in controls, which is in the same range as published data in patients with PiD [13].

In the striatum, 4R/3R mRNA ratios were higher in both patients with mainly 3R-tau aggregates (ALZ_441_005 and ALZ_596_006) (136% and 139% increase, respectively) and lower (74%) for the patient with mainly 4R-tau aggregates (EXT_1998_001) as compared with the controls mean value (Supplementary Fig. 5).

In vitro seeding experiments

All homogenates derived from samples containing misfolded tau induced the aggregation of the endogenous tau RD P301S proteins expressed by the biosensor (Fig. 5; Supplementary Fig. 6). The intracellular aggregates of tau proteins observed in biosensor cells was of different types: some aggregates were granular (types 1 and 2), while others appeared larger and denser (types 3 and 4; Fig. 5a). Morphological features of induced aggregates of three *MAPT* duplication carriers (ALZ_441_005, ALZ_596_006 and EXT_1998_001) showed dense/granular ratios between those induced by homogenates of a PiD and a PSP control (Fig. 5b), at both extremes. Indeed, the seeding-competent homogenates derived from ALZ_441_005 and PiD cases led to a majority of granular aggregates of tau proteins, that represented respectively 66.44% [95% CI 58.86; 74.02] and 67.35% [95% CI 59.77; 74.93] of total aggregates (*Z*-test comparison to the null hypothesis of equal proportions: $p < 0.0001$ for ALZ 441_005 and PiD cases, as shown in Fig. 5b). Interestingly, dense/granular ratios did not differ significantly between ALZ_441_005 and the PiD case (Fig. 5c). Conversely, samples obtained from EXT_1998_001 and PSP cases both induced a majority of dense aggregates, reaching a proportion of 63.83% [95% CI 55.90;71.76] and 76.97% [95%CI: 70.28;83.67], *Z*-test comparison to the null hypothesis of equal proportions: $p = 0.0014$ for EXT_1998_001 case and $p < 0.0001$ for PSP case, as shown in Fig. 5b). Finally, the samples obtained from ALZ_596_006 showed an intermediate proportion of dense/granular aggregates (proportion of dense aggregates: 56.21% [95% CI 48.73; 63.69]; *Z*-test comparison to the null hypothesis of equal proportions: $p = 0.1239$).

Discussion

The biological, imaging and neuropathological data presented here definitely settle one issue: the 17q21.31 duplication causes a primary tauopathy showing various combinations of well-characterized primary tauopathies, and not an atypical form of AD. Previous CSF biomarker data suggesting an Aβ pathology in 3/4 *MAPT* duplication carriers were not supported by a reassessment in one patient and more recent data obtained in two additional patients in whom Aβ levels were in the normal range. Furthermore, all three amyloid PET scans were negative; there were no senile plaques at neuropathological examination and minimal Aβ staining was present in only one case. We further ensured that no Aβ oligomers were detected, ruling out any involvement of this peptide in the pathology. Of note, the case reported by Alexander et al. [1] showed asymmetric TDP-43 deposits. We hypothesize that it could be co-incidental in this case, as none of our patients showed such immuno-reactivity, even though only one hemisphere was examined in all four cases.

Clinically, we identified eight patients presenting with episodic memory impairment following a profile observed in typical AD [8] with or without behavioral symptoms upon presentation, on one side, and one patient with an isolated atypical extrapyramidal presentation resembling the one observed in progressive supranuclear palsy (PSP), on the other side. These clinical presentations appear as two extremes, belonging to a spectrum. That hypothesis is supported by (i) the association, in the remaining case with an atypical extrapyramidal syndrome upon presentation, of an early memory impairment that worsened during follow up and (ii) the fact that three cases with memory impairment upon presentation also exhibited significant dopaminergic nigrostriatal neuronal depletion as observed on DaTscan imaging despite normal physical examination, thus suggesting partial alteration of dopaminergic pathways however insufficient to induce the emergence of extrapyramidal signs as described in premotor Parkinson's disease stages [25]. Interestingly, in the family described by Alexander et al.[1], both the proband and his sister presented memory and behavioral impairment, with neuropsychological assessments and MRI consistent with a diagnosis of probable AD, but also exhibited mild to moderate extrapyramidal symptoms upon examination.

Neuropathological examination combining immunohistochemical and biochemical analyses supports such a continuum by showing that different tau isoforms formed aggregates among the four examined brains. In one case with a cognitive and behavioral disorder presentation (ALZ_441_005), we observed widespread tau deposits in the hippocampus and neocortex, which were mainly composed of 3R-tau as in PiD although globular inclusions were Gallyas positive and Bielschowsky negative in the striatum and frontal cortex. Thus, this case harbors a novel variety of Pick body-like inclusions in addition to those already associated with some *MAPT* pathogenic variants [2, 19, 26]. In contrast, in the case presenting with isolated atypical extrapyramidal syndrome (EXT_2000_001), the picture was reversed: we observed tau aggregates mainly located in subcortical regions, which were exclusively composed of 4R-tau protein isoforms. Those two cases may be seen as the extremes of the spectrum: between those

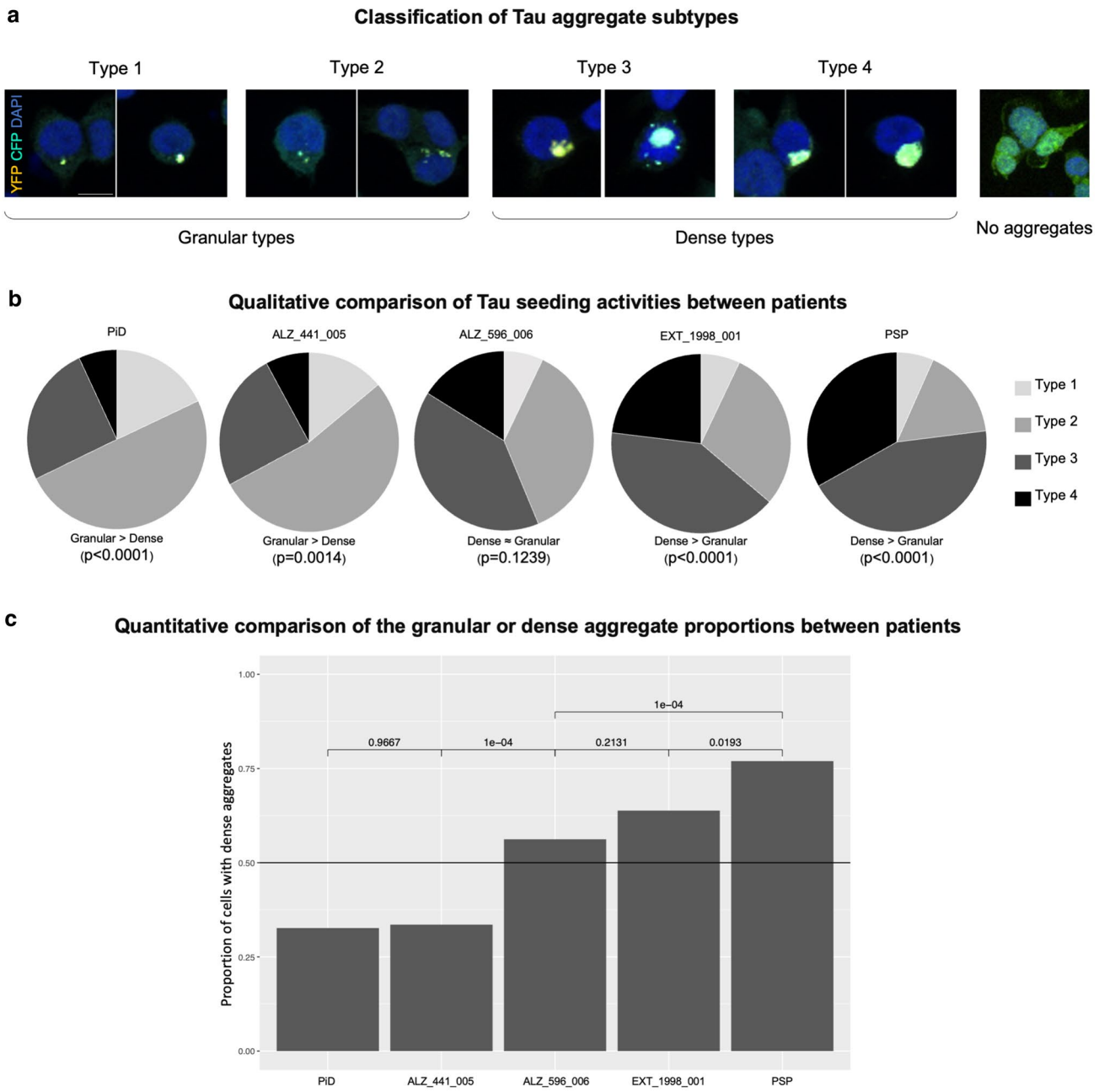

Fig. 5 In vitro characterization of tau seeding activity in the striatum of *MAPT* duplication cases in a cell biosensor. HEK cells expressing tau RD P301S coupled with fluorochromes (YFP or CFP) were exposed to brain homogenates normalized for total tau proteins, obtained from the striatum of a control case and of three *MAPT* duplication cases, pons of a PSP case and frontal cortex of a PiD case. **a** Illustration of the four types of tau aggregates. Type 1: unique and small grain (~10% of cell volume or less); Type 2: multiple granules of homogeneous size; Type 3: multiple granules associated with a larger dense core; Type 4: large and dense aggregate (~30% of cell volume or more). Representative confocal images with max YFP (yellow), CFP (cyan) and DAPI (blue) intensity projections from a stack covering all the cells contained in the field (scale bar: 10 µm); no aggregates: example of cells devoid of any aggregates in HEK cells exposed to control brain homogenate, showing diffuse YFP/CFP positive immunofluorescent staining due to non-aggregated tau-RD **b** Mean percentages of each type of tau aggregates observed for each case, obtained from three independent experiments in which a total of 50 ± 10 YFP/CFP positive cells were analyzed per condition. Proportions of "granular" (type 1 + type 2) and "dense" types of aggregates (type 3 + type 4) were compared to the null hypothesis of equal proportion using a *Z*-test for proportions. **c** Proportion of cells with dense aggregates. Comparison between two individuals using a *Z*-test for proportions

two extremes, patient EXT_1998_001, who exhibited an akinetic-rigid syndrome associated with a severe memory deficit, showed a mixed 3R/4R tauopathy, albeit with 4R-tau predominant deposits in the striatum and frontal cortex. The clinical picture, the 4R-tau predominance, the presence of 3R-tau accumulation in the subcortical nuclei is reminiscent of the case published by Alexander et al. [1]. In the last case (ALZ_596_006), closer to the dementia side, a mixed 3R/4R tauopathy similar to that seen in AD was found with severe involvement of the medial region of the temporal lobe.

Overall, *MAPT* duplication can thus lead to a spectrum of primary tauopathies with 3R- or 4R-tau predominant aggregates. Our observations suggest that 4R-tau deposits involve together basal nuclei, brainstem and basal ganglia, and are associated with motor symptoms. On the other hand, 3R-tau predominant cortical inclusions were associated with Pick-like inclusions. Those conclusions, based on the analysis of a small number of cases, obviously await confirmation by further studies.

Of note, in vivo tau PET imaging could reflect neuropathological heterogeneity of the tau pathology. Postmortem studies showed that the affinity of the tau tracer for non-AD tau lesions may be lower than that for AD tauopathy, with low or absent binding of [^{18}F]-Flortaucipir to tau straight filaments [17]. The distinct tau PET binding profiles between ALZ_596_006, and ROU_1373_001 could reflect a qualitative rather than a quantitative difference of the tau pathology, with a possible different mixed 3R/4R tauopathy in ALZ_596_001, whose tau tracer uptake was clearly increased in the temporal lobes. The tau tracer binding was far less pronounced in ROU_1373_001, who had nevertheless a similar clinical presentation, disease duration, and FDG-PET pattern. This could reflect a different type of tau lesions for which the tracer has less affinity.

We sought to identify a putative correlation between the preferential accumulation of 4R- or 3R-tau and the relative expression of tau transcripts. Focusing on the striatum where either 4R or 3R-predominant tau aggregates were present in patients, we failed to find a positive correlation with 4R/3R mRNA ratios. Rather, the relative proportion of 4R-containing transcripts was moderately increased in patients ALZ_441_005 and ALZ_596_006 with 3R-tau aggregates whereas the converse was observed in patient EXT_1998_001 with 4R deposits. Consistent with previous findings in PSP and PiD patients [13], the preferential accumulation of 4R- or 3R-tau aggregates is neither driven by the corresponding preferential expression of the 4R or 3R-encoding transcripts, nor by the *MAPT* haplotype associated with the duplication. It has been suggested, although this claim remains controversial [28], that the *MAPT* H1 haplotype [3] or sub-haplotypes [18], is associated with increased expression of 4R tau-encoding transcripts. Accumulation of 3R-tau in ALZ_441_005 occurred in the 2H1-1H2 background whereas accumulation of 4R-tau in EXT_1998_001 occurred in the 1H1-2H2 background: only one H1 haplotype was thus present in a case with 4R-tau predominant accumulation while they were two in a case in which 3R-tau was the preferential isoform, in contradiction with the hypothetical role of the H1 haplotype. Finally, the search of rare or common variants in exon 10 and surrounding splicing regions, which could have influenced the 3R/4R tau mRNA ratios remained negative. We conclude that the shift toward 3R or 4R-tau predominant pathology and the topography of lesions do not appear to be directly related to a change in the balance between the corresponding transcripts.

Local factors influencing availability or aggregation properties of different tau isoforms might explain why, in the general context of tau overexpression, aggregates are preferentially formed of 3R- or 4R-tau in discrete brain regions of a same individual. The striking inter-individual differences in the composition of aggregates observed in identical brain regions suggest, however, that this process could also be driven by the formation of different pathogenic seeds: peculiar sets of 3R or 4R misfolded tau proteins could aggregate in specific parts of the brain and subsequently spread in other cerebral regions along anatomically connected networks [5]. Tau pathology located in the striatum of ALZ_441_005, ALZ_596_006 and EXT_1998_001 cases induced different types of tau aggregates in a biosensor cell line expressing tau RD P301S (4R-tau): the striatum of ALZ_441_005 containing 3R-tau inclusions mainly led to granular aggregates (similarly to a PiD homogenate), whereas the striatum of EXT_1998_001 presenting 4R-tau inclusions mostly resulted in dense aggregates (as observed with a PSP homogenate). The striatum of ALZ_596_006, containing a mixture of 3R- and 4R-tau lesions, seeded the formation of granular and dense aggregates in similar proportions. Those morphological features were independent of the sample seeding potential, as tau seeding activity appeared higher in ALZ_441_005 and PSP homogenates than in EXT_1998_001 and PiD samples, after a total tau normalization (Supplementary Fig. 6). Our results thus support the hypothesis of different seeds among *MAPT* duplication cases. In the context of moderate *MAPT* overexpression related to the duplication, tau monomers could adopt different abnormal conformations leading to several seed competent species. Depending on the "strains", mainly 3R or 4R-tau could be preferentially incorporated, leading to various protein assemblies, resulting ultimately in different pathologies characterized by fibril morphology, cellular type specificity and anatomical spreading patterns. Also supporting this hypothesis, it has recently been shown that stochastic misfolding of tau conformers occurs in brain tissues of

patients carrying the same P301L *MAPT* mutation, followed by templated conversion of native monomers [7].

In summary, we have identified different types of *MAPT* duplication carriers exhibiting, at least in early stages of their diseases, different cognitive or motor symptoms related either to cortical or subcortical dysfunctions and characterized by the accumulation of different tau isoforms. Given the diversity of clinical and imaging presentations and the simplicity of the genetic test, we suggest searching *MAPT* duplications in all cases with early-onset idiopathic neurodegenerative dementia or early-onset idiopathic atypical extrapyramidal syndromes. They should also be sought when neuropathologically identified primary tauopathies are not related to *MAPT* mutations, particularly when the unusual constellation of tau pathology cannot be clearly put in one of the boxes of currently described primary tauopathies.

Supplementary Information The online version contains supplementary material available at https://doi.org/10.1007/s00401-021-02320-4.

Acknowledgements This work was supported by Fondation pour la Recherche Médicale (Equipe FRM DEQ20170336711). Two of the neuropathological cases described in this paper (ALZ_441_005 and ALZ_596_006) have been collected by the Neuro-CEB brain bank, Paris, France. We thank Luc Buée for helpful advices and Gabor Kovacs for sharing unpublished data. We thank the technical team at Raymond Escourolle neuropathology department. We thank the ICM-Quant core facility, Paris Brain Institute (ICM). Two patients were included in the Shatau7-Imatau study (NTC025768210). MS, JL and MB acknowledge the chemical/radiopharmaceutical and nursing staff of the Service Hospitalier Frederic Joliot for the synthesis of [11C]-PIB and [18F]-AV-1451 and patient management. MS, JL and MB are also indebted to AVID Radiopharmaceuticals, Inc., for their support in supplying the AV-1451 precursor and chemistry production advice. This study was cofunded by the French Ministry of Health grant (PHRC-2013-0919), CEA, Fondation pour la recherche sur Alzheimer, Institut de recherche internationale Servier, France-Alzheimer.

Declarations

Conflict of interest The authors have nothing to disclose in relation to this article.

References

1. Alexander J, Kalev O, Mehrabian S, Traykov L, Raycheva M, Kanakis D et al (2016) Familial early-onset dementia with complex neuropathologic phenotype and genomic background. Neurobiol Aging 42:199–204
2. Bronner IF, ter Meulen BC, Azmani A, Severijnen LA, Willemsen R, Kamphorst W et al (2005) Hereditary Pick's disease with the G272V tau mutation shows predominant three-repeat tau pathology. Brain 128:2645–2653
3. Caffrey TM, Joachim C, Paracchini S, Esiri MM, Wade-Martins R (2006) Haplotype-specific expression of exon 10 at the human MAPT locus. Hum Mol Genet 15:3529–3537
4. Chen Z, Chen JA, Shatunov A, Jones AR, Kravitz SN, Huang AY et al (2019) Genome-wide survey of copy number variants finds MAPT duplications in progressive supranuclear palsy. Mov Dis 34:1049–1059
5. Clavaguera F, Bolmont T, Crowther RA, Abramowski D, Frank S, Probst A et al (2009) Transmission and spreading of tauopathy in transgenic mouse brain. Nat Cell Biol 11:909–913
6. Dan A, Takahashi M, Masuda-Suzukake M, Kametani F, Nonaka T, Kondo H et al (2013) Extensive deamidation at asparagine residue 279 accounts for weak immunoreactivity of tau with RD4 antibody in Alzheimer's disease brain. Acta Neuropathol Commun 1:54
7. Daude N, Kim C, Kang S-G, Eskandari-Sedighi G, Haldiman T, Yang J et al (2020) Diverse, evolving conformer populations drive distinct phenotypes in frontotemporal lobar degeneration caused by the same MAPT-P301L mutation. Acta Neuropathol 139:1045–1070
8. Dubois B, Feldman HH, Jacova C, Hampel H, Molinuevo JL, Blennow K et al (2014) Advancing research diagnostic criteria for Alzheimer's disease: the IWG-2 criteria. Lancet Neurol 13:614–629
9. Furman JL, Holmes BB, Diamond MI (2015) Sensitive Detection of Proteopathic Seeding Activity with FRET Flow Cytometry. J Vis Exp. https://doi.org/10.3791/53205
10. Godefroy O, Azouvi P, Robert P, Roussel M, LeGall D, Meulemans T et al (2010) Dysexecutive syndrome: diagnostic criteria and validation study. Ann Neurol 68:855–864
11. Holmes BB, Furman JL, Mahan TE, Yamasaki TR, Mirbaha H, Eades WC et al (2014) Proteopathic tau seeding predicts tauopathy in vivo. PNAS 111:E4376–E4385
12. Hooli BV, Kovacs-Vajna ZM, Mullin K, Blumenthal MA, Mattheisen M, Zhang C et al (2014) Rare autosomal copy number variations in early-onset familial Alzheimer's disease. Molecular Psy 19:676–681
13. Ingelsson M, Ramasamy K, Russ C, Freeman SH, Orne J, Raju S et al (2007) Increase in the relative expression of tau with four microtubule binding repeat regions in frontotemporal lobar degeneration and progressive supranuclear palsy brains. Acta Neuropathol 114:471–479
14. Kovacs GG (2015) Invited review: Neuropathology of tauopathies: principles and practice. Neuropathol Appl Neurobiol 41:3–23
15. Le Guennec K, Quenez O, Nicolas G, Wallon D, Rousseau S, Richard A-C et al (2017) 17q21.31 duplication causes prominent tau-related dementia with increased MAPT expression. Molecular Psy 22:1119–1125
16. Lesné S, Koh MT, Kotilinek L, Kayed R, Glabe CG, Yang A et al (2006) A specific amyloid-beta protein assembly in the brain impairs memory. Nature 440:352–357
17. Marquié M, Normandin MD, Vanderburg CR, Costantino IM, Bien EA, Rycyna LG et al (2015) Validating novel tau positron emission tomography tracer [F-18]-AV-1451 (T807) on postmortem brain tissue. Ann Neurol 78:787–800
18. Myers AJ, Pittman AM, Zhao AS, Rohrer K, Kaleem M, Marlowe L et al (2007) The MAPT H1c risk haplotype is associated with increased expression of tau and especially of 4 repeat containing transcripts. Neurobiol Dis 25:561–570
19. Neumann M, Schulz-Schaeffer W, Crowther RA, Smith MJ, Spillantini MG, Goedert M et al (2001) Pick's disease associated with the novel Tau gene mutation K369I. Ann Neurol 50:503–513
20. Rösler TW, Marvian AT, Brendel M, Nykänen N-P, Höllerhage M, Schwarz SC et al (2019) Four-repeat tauopathies. Prog Neurobiol 180:101644
21. Rovelet-Lecrux A, Hannequin D, Guillin O, Legallic S, Jurici S, Wallon D et al (2010) Frontotemporal dementia phenotype associated with MAPT gene duplication. JAD 21:897–902

22. Sahara N, Kimura T (2018) Biochemical properties of pathology-related tau species in tauopathy brains: an extraction protocol for tau oligomers and aggregates. Methods Mol Biol 1779:435–445
23. Sarazin M, Berr C, Rotrou JD, Fabrigoule C, Pasquier F, Legrain S et al (2007) Amnestic syndrome of the medial temporal type identifies prodromal AD: a longitudinal study. Neurology 69:1859–1867
24. Scheltens P, Barkhof F, Leys D, Pruvo JP, Nauta JJ, Vermersch P et al (1993) A semiquantative rating scale for the assessment of signal hyperintensities on magnetic resonance imaging. J Neurol Sci 114:7–12
25. Sierra M, Martínez-Rodríguez I, Sánchez-Juan P, González-Aramburu I, Jiménez-Alonso M, Sánchez-Rodríguez A et al (2017) Prospective clinical and DaT-SPECT imaging in premotor LRRK2 G2019S-associated Parkinson disease. Neurology 89:439–444
26. Tacik P, DeTure MA, Carlomagno Y, Lin W, Murray ME, Baker MC et al (2017) FTDP-17 with Pick body-like inclusions associated with a novel tau mutation, p. E372G. Brain Pathol 27:612–626
27. Thierry M, Boluda S, Delatour B, Marty S, Seilhean D, Network BN-CN et al (2020) Human subiculo-fornico-mamillary system in Alzheimer's disease: Tau seeding by the pillar of the fornix. Acta Neuropathol 139:443–461
28. Trabzuni D, Wray S, Vandrovcova J, Ramasamy A, Walker R, Smith C et al (2012) MAPT expression and splicing is differentially regulated by brain region: relation to genotype and implication for tauopathies. Hum Mol Genet 21:4094–4103
29. Uchihara T, Kondo H, Ikeda K, Kosaka K (1995) Alzheimer-type pathology in melanin-bleached sections of substantia nigra. J Neurol 242:485–489
30. Yamamoto T, Hirano A (1986) A comparative study of modified Bielschowsky, bodian and thioflavin S stains on Alzheimer's neurofibrillary tangles. Neuropath Appl Neuro 12:3–9

Authors and Affiliations

David Wallon[1] · Susana Boluda[2,3] · Anne Rovelet-Lecrux[4] · Manon Thierry[2,3] · Julien Lagarde[5,6,7] · Laetitia Miguel[4] · Magalie Lecourtois[4] · Antoine Bonnevalle[1] · Marie Sarazin[5,6,7] · Michel Bottlaender[7,8] · Mathieu Mula[3] · Serge Marty[2] · Natsuko Nakamura[2] · Catherine Schramm[4] · François Sellal[9] · Thérèse Jonveaux[10] · Camille Heitz[11] · Isabelle Le Ber[12,13] · Stéphane Epelbaum[14,15] · Eloi Magnin[14,15] · Aline Zarea[1] · Stéphane Rousseau[4] · Olivier Quenez[4] · Didier Hannequin[1] · Florence Clavaguera[2] · Dominique Campion[4] · Charles Duyckaerts[2,3] · Gaël Nicolas[4]

1 Normandie Univ, UNIROUEN, Inserm U1245, CHU Rouen, Department of Neurology and CNR-MAJ, F-76000 Rouen, France

2 Sorbonne Université, INSERM, CNRS U1127, Institut du Cerveau, ICM, Paris, France

3 AP-HP, Hôpital de La Pitié-Salpêtrière, Laboratoire de Neuropathologie R. Escourolle, Paris, France

4 Normandie Univ, UNIROUEN, Inserm U1245, CHU Rouen, Department of Genetics and CNR-MAJ, F-76000 Rouen, France

5 Department of Neurology of Memory and Language, GHU Paris Psychiatrie & Neurosciences, Hôpital Sainte Anne, F-75014 Paris, France

6 Université de Paris, 75006 Paris, France

7 Université Paris-Saclay, BioMaps, Service Hospitalier Frederic Joliot, CEA, CNRS, Inserm, F-91401 Orsay, France

8 UNIACT, Neurospin, CEA, 91191 Gif-sur-Yvette, France

9 Department of Neurology, Hôpitaux Civils de Colmar and INSERM U-1118, School of Medicine, Strasbourg University, Strasbourg, France

10 CMRR Department of Neurology, Nancy University Hospital, Laboratoire Lorraine de Psychologie et de Neurosciences de la Dynamique des Comportements 2LPN EA7489 Lorraine University, Nancy, France

11 Neurology Department, Hôpital Universitaire de Nîmes, Nîmes, France

12 Sorbonne Universités, UPMC Univ Paris 06, Inserm U1127, CNRS UMR 7225, Institut du Cerveau et la Moelle Epinière(ICM), AP-HP - Hôpital Pitié-Salpêtrière, Paris, France

13 Reference Centre for Rare or Early Dementias, IM2A, Département de Neurologie, AP-HP, Hôpital Pitié-Salpêtrière, Paris, France

14 Centre Mémoire Ressources et Recherche (CMRR), Centre Expert Parkinson (CEP), Service de Neurologie, CHRU Besançon, 25000 Besançon, France

15 Neurosciences Intégratives et Cliniques UR481, Univ. Bourgogne Franche-Comté, 25000 Besançon, France